BIOCHEMISTRY
including biophysical chemistry & molecular biology

Article

pubs.acs.org/biochemistry

De Novo Design of an Artificial Bis[4Fe-4S] Binding Protein

Anindya Roy,[†] Iosifina Sarrou,[†] Michael D. Vaughn,[†] Andrei V. Astashkin,[‡] and Giovanna Ghirlanda*[,†]

[†]Department of Chemistry and Biochemistry, Arizona State University, Tempe, Arizona 85287-1604, United States

[‡]Department of Chemistry and Biochemistry, University of Arizona, Tucson, Arizona 85721, United States

Supporting Information

ABSTRACT: In nature, protein subunits containing multiple iron−sulfur clusters often mediate the delivery of reducing equivalents from metabolic pathways to the active site of redox proteins. The *de novo* design of redox active proteins should include the engineering of a conduit for the delivery of electrons to and from the active site, in which multiple redox active centers are arranged in a controlled manner. Here, we describe a designed three-helix protein, DSD-bis[4Fe-4S], that coordinates two iron−sulfur clusters within its hydrophobic core. The design exploits the pseudo two-fold symmetry of the protein scaffold, DSD, which is a homodimeric three-helix bundle. Starting from the sequence of the parent peptide, we mutated eight leucine residues per dimer in the hydrophobic core to cysteine to provide the first coordination sphere for cubane-type iron−sulfur clusters. Incorporation of two clusters per dimer is readily achieved by *in situ* reconstitution and imparts increased stability to thermal denaturation compared to that of the apo form of the peptide as assessed by circular dichroism-monitored thermal denaturation. The presence of [4Fe-4S] clusters in intact proteins is confirmed by UV−vis spectroscopy, gel filtration, analytical ultracentrifugation, and electron paramagnetic resonance spectroscopy. Pulsed electron−electron double-resonance experiments have detected a magnetic dipole interaction between the two clusters ∼0.7 MHz, which is consistent with the expected intercluster distance of 29−34 Å. Taken together, our data demonstrate the successful design of an artificial multi-iron−sulfur cluster protein with evidence of cluster−cluster interaction. The design principles implemented here can be extended to the design of multicluster molecular wires.

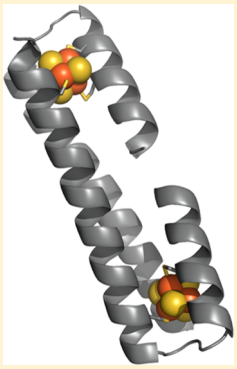

[Fe-S] cluster proteins make up one of the most abundant and functionally pliable classes of proteins: they carry out a wide variety of biological functions, including catalysis, oxygen sensing, and electron transfer.[1,2] The chemical properties of the [Fe-S] clusters, such as low redox potential (with the exception of high-potential iron−sulfur proteins, HIPIP) and high oxygen sensitivity, their prevalence, and their structural and functional flexibility, suggest that they emerged during early evolution.[3,4] Most frequently, [Fe-S] clusters act as donors or acceptors of electrons over a wide range of potentials, and they are organized in protein-embedded redox chains that function as relays for the transfer of electrons from soluble protein partners to catalytic centers in complex, often multiunit, proteins.[5−9]

The most common type of [Fe-S] cluster, the [4Fe-4S] cubanelike structure, is generally coordinated by four cysteines in a variety of protein folds, often in a combination of loops and secondary structure elements.[3] A common fold is that of the ferredoxins, small soluble electron carrier proteins that can contain one or two clusters coordinated by four conserved cysteines each.[3,10] The two-cluster ferredoxin-like fold is also found in the PsaC subunit of Photosystem I[11] and in hydrogenases as part of the accessory iron−sulfur cluster binding domain, which regulates long-range electron transfer to and from the active site (H-cluster).[8,12−14]

Over the years, a substantial amount of scientific effort has been dedicated to elucidating the structure−function relationships of different clusters with their protein counterparts in natural and *de novo*-designed model systems. Model proteins designed to coordinate an iron−sulfur cluster generally utilize loop regions to accommodate the cluster, with a sequence and topology resembling those found in most of the natural proteins.[15−18] Computational approaches have been used to position an idealized cluster into a designed four-helix coiled coil[19,20] or into the structure of natural proteins.[21] These models were designed to contain a single iron−sulfur cluster, either isolated within the protein scaffold or in the proximity of a second cofactor.[22,23] When functioning as electron conduits, however, iron−sulfur clusters are generally arranged in chains of two or more.[5−9]

As a first step toward constructing bioinspired functional redox proteins encompassing an electron transfer domain and a catalytic domain,[24,25] we have engineered a model system that contains two [4Fe-4S] clusters embedded in the hydrophobic core of a *de novo*-designed helical three-helix bundle. We present here the design, synthesis, and characterization of this model system, DSD-bis[4Fe-4S], demonstrating for the first time the incorporation of two clusters at a defined distance. This approach can be extended to the design of other systems, in which the intercluster distance can be modulated by exploiting the geometric properties of α-helical coiled coils.[19,26,27]

Received: August 29, 2013
Revised: October 2, 2013
Published: October 3, 2013

MATERIALS AND METHODS

Chemicals. Chemicals were purchased from Sigma-Aldrich; Fmoc-protected amino acids for solid phase peptide synthesis were purchased from Novabiochem. All reactions were performed in an inert environment using a Schlenk line or in a glovebox (Coy Scientific), unless otherwise noted. All buffers and solutions were degassed extensively by being purged with N_2 prior to their transfer to the glovebox.

Protein Design. Models of DSD-4Cys and DSD-bis[4Fe-4S] were built in MacPyMol[28] starting from the coordinates of DSD [Protein Data Bank (PDB) entry 1G6U]. Leucines 9, 12, 22, and 43 in DSD were mutated to cysteine, and side chain orientations were selected among the backbone-dependent favorable rotamers in MacPyMol. The disembodied [4Fe-4S] cluster and four cysteines that form the primary coordination sphere were obtained from *Thermotoga maritima* tryptophanyl tRNA synthase (PDB entry 2G36) and manually docked onto DSD-4Cys using pairwise alignment in MacPyMol. Finally, new bonds were created using the Build function. The models of DSD-4Cys, DSD-bis[4Fe-4S], and the original DSD structure were analyzed with Q-SiteFinder,[29] which identifies and measures the volume of cavities using PDB entries as input.

Peptide Synthesis and Purification. DSD-4Cys, which is comprised of 49 amino acids, was synthesized on a Liberty microwave-assisted solid phase peptide synthesizer (CEM). Peptide synthesis was performed using a standard Fmoc/t-Bu/Trt protecting strategy on a Rink amide resin; the N-terminus of the peptide was acetylated. Cleavage from the resin and simultaneous removal of side chain protecting groups was achieved by treatment with 94% TFA, 2.5% water, 2.5% EDT, and 1% TIS. The crude peptide was purified by high-performance liquid chromatography on a C-18 semipreparative column (Vydac, 1 cm × 25 cm), using gradient elution with solvent system A (100% water and 0.1% TFA) and solvent system B (95% acetonitrile, 5% water, and 0.1% TFA) at a flow rate of 4 mL/min. Peptide purity was confirmed by reinjecting appropriate fractions on an analytical C-18 column; the molecular mass of the peptide was verified by matrix-assisted desorption ionization time-of-flight (MALDI-TOF) mass spectrometry. Peptides used for further experiments were >99% pure.

Direct Incorporation of the [4Fe-4S] Cluster into the Synthesized Peptides. All the reactions were performed in an anaerobic chamber (Coy Scientific) under an inert atmosphere. Cluster incorporation was performed following an established protocol.[16] Briefly, a 120 μM solution of DSD-4Cys peptide in 100 mM Tris-HCl (pH 8.5) and 2 M urea was treated with 0.8% (v/v) BME for 2 h. To this solution were added iron(III) chloride ($FeCl_3$) and a freshly prepared solution of sodium sulfide (Na_2S) in water in 30 min intervals to a final concentration of 30 mM. The resulting dark brown solution was incubated overnight at 4 °C under N_2. The reaction mixture was then passed through a PD10 G25 desalting column (GE Healthcare) pre-equilibrated with 50 mM Tris-HCl buffer (pH 7.5) to exclude all nonprotein, low-molecular mass contaminants and salts. Appropriate fractions were collected in 1 mL increments and subjected to characterization.

UV−Vis Spectroscopy. UV−vis spectra were recorded on a Perkin-Elmer Lambda-35 spetrophotomether under anaerobic conditions using a sealed cuvette with a path length of 1 cm.

Gel Filtration. The oligomerization states of DSD-4Cys and DSD-bis[4Fe-4S] were determined on a G-25 gel filtration column using an Agilent Technologies 1260 Insight FPLC system. The apo peptide was treated with a 10-fold molar excess of DTT at 4 °C to prevent disulfide formation. DSD-bis[4Fe-4S] was kept under anaerobic conditions prior to injection. The assignment of the elution peak to the dimer was confirmed by analytical ultracentrifugation (Supporting Information).

Circular Dichroism (CD) Spectroscopy. CD spectroscopy of the apo and holo peptides was conducted on a JASCO J-815 spectropolarimeter. Spectra were recorded from 240 to 190 nm in 1 nm increments at protein concentrations of 0.050 and 0.025 mM in 10 mM Tris-HCl (pH 7.5) using a quartz cuvette with a path length of 1 mm; the final spectra are the average of three data sets. Thermal unfolding curves were monitored by following the CD signal at 222 nm as a function of temperature from 4 to 96 °C. Holo DSD-bis[4Fe-4S] peptide samples were handled in an airtight cuvette to exclude air during the course of the experiment. CD spectra of DSD-4Cys were recorded in the presence of excess reducing agent (TCEP) to prevent oxidation of the cysteine side chains.

Electron Paramagnetic Resonance (EPR) Spectroscopy. Appropriate fractions from the PD10 column were concentrated using a centrifuge concentrator with a molecular mass cutoff of 3000 Da (GE Healthcare). The pH values of the samples were then adjusted to pH 10 by addition of 1 M glycine buffer, and the samples were reduced by addition of 100 mM $Na_2S_2O_4$ in 1 M glycine buffer (pH 10). Aliquots (150 μL) of the reduced samples were transferred to quartz EPR tubes, flash-frozen by immersion in liquid nitrogen, and stored at 77 K until EPR characterization.

Continuous wave (CW) EPR experiments were performed on the X-band EPR spectrometer Elexsys E500 (Bruker). Pulsed EPR experiments were performed on a home-built broadband (2−18 ∪ 26−40 GHz) pulsed EPR spectrometer[30] at microwave (mw) frequencies of ∼9.6 GHz. The measurement temperature was 15 K. Detailed experimental conditions are given in the figure captions.

Cluster Quantification. For each preparation, the percentage yield of cluster incorporation was estimated by UV−vis, using an ε of 5500 M^{-1} cm^{-1} per protein and an ε of 16000 M^{-1} cm^{-1} per cluster at 410 nm; depending on preparations, the yield of incorporation ranged between 80 and 100%.[31] Cluster incorporation was assessed quantitatively by measuring independently the concentration of iron and of peptide in identical samples. First, DSD-bis[4Fe-4S] samples were further purified by anion exchange chromatography on a Q-Sepharose FF column (GE Healthcare), using 100 mM Tris (pH 8.5) as equilibration buffer and 100 mM NaCl and 100 mM Tris (pH 8.5) as elution buffer. The samples were split into two portions: one was used to measure the peptide concentration by amino acid analysis (Proteomics Department, University of California, Davis, CA), and the second was used to determine the iron concentration by a ferrozine assay.[32] Incorporation of the EPR active, reduced cluster was determined by EPR spin quantification. Briefly, a concentrated DSD-bis[4Fe-4S] sample was divided into two parts, one of which was submitted for peptide concentration determination by amino acid analysis. The second portion was prepared for EPR spectroscopy as described above and subjected to spin quantification by comparing the double integral of the CW EPR spectrum of $[4Fe-4S]^+$ recorded at 7 K with the spectrum of 5 mM Cu(II)

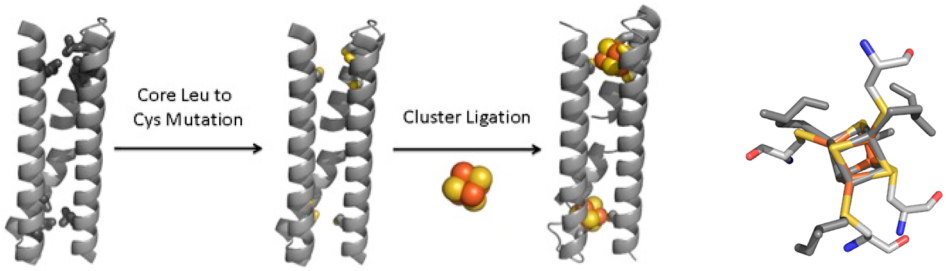

DSD: SLAALKSELQALKKEGFSPEELAALESELQALEKKLAALKSKLQALKG

DSD-4Cys: SLAALKSE**C**QA**C**KKEGFSPEE**C**AALESELQALEKKLAALKSK**C**QALKGW

Figure 1. Design of DSD-bis[4Fe-4S]. In the top panel, the crystal structure of DSD (PDB entry 2G6U) serves as a starting point. The [4Fe-4S] cluster from *T. maritima*, including the four cysteines comprising its first coordination sphere, was docked in the core of DSD. Appropriate core leucine residues in the hydrophobic core were mutated to cysteines. The first coordination sphere of DSD-bis[4Fe-4S] displays an excellent agreement with the natural coordination sphere of the cluster. The bottom panel shows sequences of DSD and DSD-4Cys. Mutations to the DSD sequence in DSD-4Cys are highlighted in bold. A tryptophan was inserted at the C-terminus to facilitate the assessment of concentration.

nitrate recorded at 21 K [at lower temperatures, the Cu(II) EPR signal was saturated even at the lowest accessible mw power of 0.2 μW]. The estimated concentration of $[4Fe\text{-}4S]^{+}$ was then compared with the DSD protein concentration evaluated using amino acid analysis for the same sample (accounting for dilutions).

RESULTS AND DISCUSSION

Design of the Model Peptide. DSD-bis[4Fe-4S] was designed by using as a scaffold a dimeric three-helix bundle originally designed to probe domain swapping (domain-swapped dimer, DSD, PDB entry 1G6U). In DSD, two identical peptides each form a helical hairpin, in which one of the helices is approximately twice the other in length. The long helices from two monomers pair up in an antiparallel manner, while the two shorter helices dock against the dimer formed by the long helices. An approximate 2-fold symmetry axis is located between the two short helices (Figure 1). The fold is stabilized by a leucine-rich hydrophobic core and by salt bridges positioned at the helix−helix interfaces to impart specificity.

The arrangement of the two monomers in DSD is reminiscent of the internal pseudo 2-fold symmetry found in two-cluster ferredoxins, which have long been thought to derive from gene duplication events and domain swapping.[4] Ferrodoxins comprise two repeats of a 29-residue sequence and adopt the so-called ferredoxin fold defined by a $\beta\alpha\beta\beta\alpha\beta$ secondary structure. In the two-cluster bacterial ferredoxins, each of the two symmetric clusters is coordinated by three sequentially contiguous cysteines contained in the loop, between the helix and the second β-sheet. A fourth distal cysteine, which is located in the helix of the second sequence repeat, completes the first coordination sphere of the cluster. The sequence motif is CXXCXXC...C. Mirroring this arrangement, we designed a binding site in which three of the coordinating cysteines belong to a monomer, while the fourth is provided by the second monomer. DSD-bis[4Fe-4S], however, differs from the ferredoxins both in its highly helical secondary structure and in its dimeric oligomerization state. To ensure a correct selection of cysteine rotamers, we docked a natural [4Fe-4S] cluster and its primary coordination sphere into the hydrophobic core of DSD. This "metal-first" approach has been successfully used to insert iron−sulfur clusters into natural and designed proteins.[19,21] We referred to the cluster found in *T. maritima* tryptophanyl tRNA synthase (PDB entry 2G36),[33] which has been used by Grzyb et al. as a starting point to model a symmetrized cluster.[19] The cluster is coordinated through a C...C...CXXC sequence motif, in which the CXXC residues are part of a helix, as assessed by backbone dihedral angles, while the two additional cysteines are found at the base of interhelix loops and are in a nonhelical conformation. The distances between the backbone atoms of the cysteines are compatible with the regular three-helix coiled coil geometry of DSD. Accordingly, once we overlaid the CXXC motif with the LXXL motif that forms the core of DSD, the Cα atoms of the two remaining cysteines overlapped with the Cα atoms of leucines forming the core of native DSD. Several core positions corresponding to different layers within the coiled coil were possible matches for the geometry of the four-cysteine motif; we selected the alignment that results in minimal clashes and supports the correct rotamers for the cysteine side chains (see Materials and Methods). We evaluated the impact of four Leu to Cys mutations and of cluster insertion on the integrity of the peptide scaffold by analyzing the models with Q-SiteFinder[29] and comparing the results to the X-ray structure of DSD (Figure S1 of the Supporting Information). This analysis revealed the presence of a 58 Å^3 cavity in the core of DSD-4Cys corresponding to the cluster binding site, and smaller pockets to the side. This central cavity is completely occupied by the [4Fe-4S] cluster in the model of DSD-bis[4Fe-4S], which presents only the small pockets to the side. DSD-bis[4Fe-4S] resembles the original DSD structure, which contains no cavities in the core, and identical side pockets.

The cluster binding site is located at one end of the bundle; because of the symmetry of the scaffold, the site is replicated in the second half (Figure 1). The sequence of the monomeric peptide contains four Leu to Cys mutations, three of which are contiguous in the sequence and a fourth one that is distal; we have named the peptide DSD-4Cys. The peptide was synthesized by solid phase peptide synthesis (SPPS) and purified as described in Materials and Methods.

Assembly of DSD-bis[4Fe-4S]. We reconstituted the clusters into the apo DSD-4Cys peptide using a well-established *in situ* synthetic procedure under anaerobic conditions.[16] Briefly, the reconstitution reaction was conducted with ferric chloride and sodium sulfide in aqueous buffer (pH 8.5) in the presence of 2-mercaptoethanol and 2 M urea that serves to partially unfold DSD-4Cys, permitting access to the cysteines located in the hydrophobic core. Cluster incorporation is

dx.doi.org/10.1021/bi401199s | *Biochemistry* 2013, 52, 7586−7594

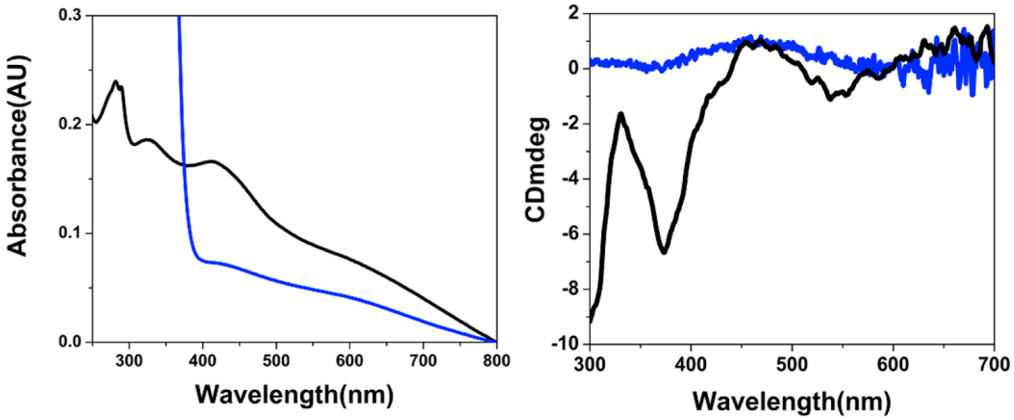

Figure 2. Optical absorption spectrum (left) of reconstituted DSD-bis[4Fe-4S] in the oxidized state (black line) showing bands at 324 and 415 nm. The reduced state (blue line) shows the loss of 415 nm absorption after reduction. Circular dichroism spectrum (right) in the visible region of reconstituted, oxidized DSD-bis[4Fe-4S] (black line). The induced dichroic absorption that corresponds to the optical absorption in the visible range indicates that the cluster is in a chiral environment. No signal is observed in the 300−700 nm range for DSD-4Cys.

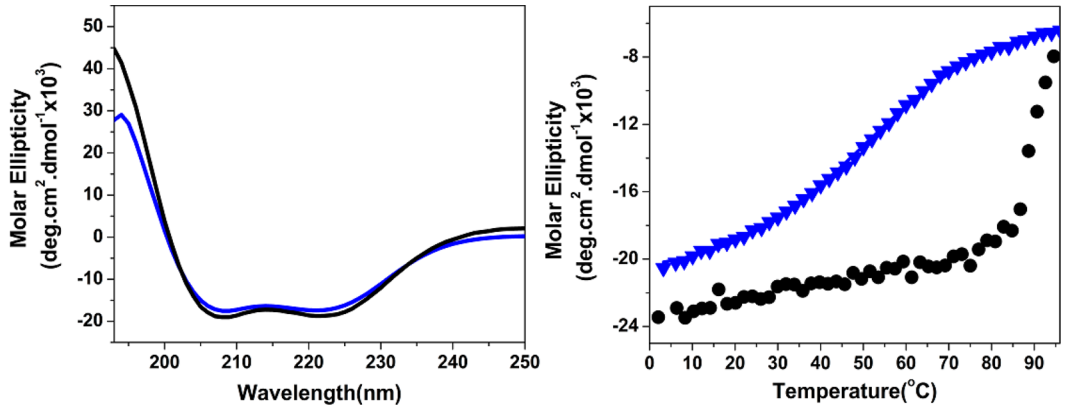

Figure 3. CD spectra (left) in the UV range recorded at 22 °C and thermal denaturation curves (right) of DSD-4Cys (blue lines) and DSD-bis[Fe4-S4] (black lines). The denaturation curves were obtained by monitoring the loss of the helical signal by CD at 222 nm while the temperature was increased.

entropically favorable and proceeds by ligand exchange between the four preorganized cysteines and the more basic 2-mercaptoethanol that initially ligate the cluster.[16,34,35]

The UV−vis spectrum of the resulting DSD-bis[4Fe-4S] protein shows broad absorptions at 415 and 360 nm, which arise from sulfur to iron charge transfer excitations in oxidized [4Fe-4S] clusters; the absorption at 415 nm disappears upon reduction with sodium dithionate (Figure 2). The positions of the maxima are red-shifted compared with those of inorganic [4Fe-4S] clusters, consistent with a cluster shielded from the aqueous environment. These spectral features and redox-dependent behavior are typical of iron−sulfur cluster proteins.[36,37] The ratio of absorbance at 410 nm to that at 280 nm is 0.76, within the range of 0.7−0.8 usually observed in natural proteins.[36,37] On the basis of these values, we estimate the peptide/cluster stoichiometry to be 1/1, consistent with a dimeric peptide coordinating two clusters. Analysis by MALDI of a preparation made at low peptide concentrations showed a broad peak corresponding to the mass of DSD-bis[4Fe-4S], two peptides, and two cubane clusters (Figure S6 of the Supporting Information).

The level of incorporation evaluated on a more concentrated preparation using the ferrozine assay was 74%, corresponding to an estimated population of at least 55% of the dimers containing two clusters.

We further characterized the redox behavior of DSD-bis[4Fe-4S] by cyclic voltammetry (Figure S5 of the Supporting Information). In the presence of 4 mM neomycin as a stabilizer, we observed a cathodic wave at −478 mV versus the standard hydrogen electrode, which is in the range observed for natural cubane-type iron−sulfur clusters.[35] However, the absence of an anodic wave indicates the electrochemical irreversibility of the process under these conditions.

Protein Folding and Stability. We verified that DSD-4Cys and DSD-bis[4Fe-4S] fold into dimers, as observed in the structure of DSD, by gel filtration, monitoring elution at wavelengths of 220, 280, and 410 nm. The two proteins have identical elution profiles dominated by a single peak at 30 min, consistent with the presence of a single species with the molecular mass of a dimer (Supporting Information). Furthermore, sedimentation velocity experiments by analytical ultracentrifugation of DSD-4Cys yielded an apparent molecular mass (12.4 kDa) in excellent agreement with that expected for a dimer (10.6 kDa) at a loading concentration of 100 μM, thus indicating that the protein forms a stable dimer in the micromolar range (Supporting Information). The sedimentation data confirm our assignment of the peaks observed in the gel filtration elution profile to dimers.

The impact of mutations on the structure of DSD in apo DSD-4Cys and in reconstituted DSD-bis[4Fe-4S] was verified

dx.doi.org/10.1021/bi401199s | *Biochemistry* 2013, 52, 7586−7594

by CD spectroscopy. Analysis of the models of DSD-4Cys and DSD-bis[4Fe-4S] shows that exchanging the hydrophobic side chain of leucine with the smaller, polar side chain of cysteine results in a polar cavity in the core of the bundle. The dimensions of the cavity calculated using Q-SiteFinder are compatible with the cubane iron−sulfur cluster; further, coordination by the cysteines to the iron−sulfur cluster stabilizes the fold and replaces hydrophobic interactions.

The secondary structure content of apo DSD-4Cys and of reconstituted DSD-bis[4Fe-4S] was evaluated by analyzing the corresponding CD spectra. Like that of DSD, both spectra contain bands at 190, 208, and 222 nm typical of α-helical proteins. The spectra are indistinguishable, indicating that the secondary structure of the protein is not distorted significantly upon insertion of the [4Fe-4S] cluster. The visible portion of the CD spectrum of DSD-bis[4Fe-4S] is dominated by a complex feature, comprising a narrow negative signal at approximately 360 nm and a broader signal centered at 560 nm, which arises from the [4Fe-4S] clusters and resembles the spectra of ferredoxins.[36,38] Such a signature for DSD-bis[4Fe-4S] corroborates the evidence of the successful incorporation of the cluster.

To further evaluate the impact of modifications on DSD in apo DSD-4Cys and in reconstituted DSD-bis[4Fe-4S], we have investigated their thermal denaturation by monitoring the decrease in the magnitude of the helical signal at 222 nm as a function of temperature. A comparison of the melting curves (see Figure 3) reveals conspicuous differences in stability. The thermal denaturation of DSD-bis[4Fe-4S] is irreversible, as partial denaturation results in a loss of the cofactor, thus precluding a rigorous thermodynamic analysis aimed at extrapolating folding parameters: the following discussion is thus limited to comparison of denaturation profiles and apparent melting points (T_m).

We chose DSD as a starting scaffold because of its remarkable thermal stability. DSD retains >90% of its helical structure at temperatures as high as 94 °C: a complete unfolding transition was observed only by subjecting DSD to thermal denaturation in the presence of 3 M guanidinium chloride.[39] Not surprisingly, substituting eight leucines per dimer with cysteines in the hydrophobic core of DSD-4Cys results in a loss of stability. In contrast to that of DSD, the thermal denaturation curve of DSD-4Cys shows unfolding even in the absence of guanidinium chloride; the protein, however, is still very stable, with an apparent T_m of 50 °C. Incorporation of the cluster into DSD-4Cys restores the thermal stability: as shown in Figure 3, DSD-bis[4Fe-4S] is more than 90% folded at 80 °C; the apparent T_m is 87 °C. As the temperature increases above 80 °C, though, the protein undergoes rapid unfolding and loses the cluster, as evident from the observation of an iron precipitate. The apparent T_m observed for DSD-bis[4Fe-4S] is remarkable for a protein of this size. Further, the trend in stability observed across the series (DSD, DSD-bis[4Fe-4S], and DSD-4Cys) reflects the packing integrity of the cores as estimated by PocketFinder (see above). Loss of stability is observed in DSD-4Cys, which contains unfilled pockets in the core.

EPR Spectroscopy. The CW EPR spectrum obtained for the DSD-bis[4Fe-4S] sample reduced with dithionite (shown in Figure 4a) exhibits principal g values of 1.879 (g_x), 1.943 (g_y), and 2.058 (g_z), with a g_{iso} of 1.965, and is similar to the spectra of $[4Fe\text{-}4S]^+$ clusters described in the literature,[35] which confirms the presence of intact [4Fe-4S] clusters bound to

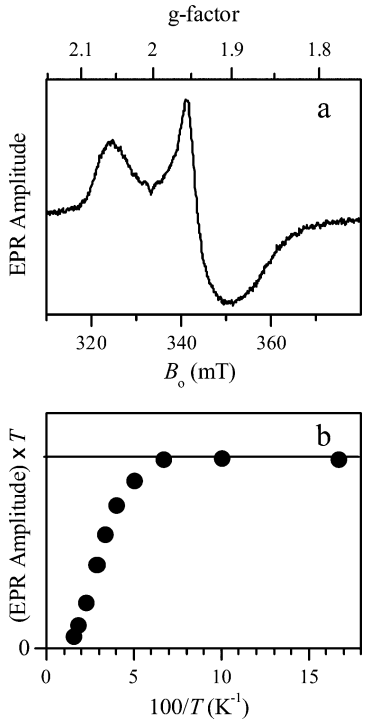

Figure 4. (a) EPR spectrum of DSD-bis[4Fe-4S] reduced with sodium dithionite. Experimental conditions: mw frequency, 9.340 GHz; mw power, 2 mW; field modulation amplitude, 0.5 mT; temperature, 15 K. (b) Temperature dependence of the EPR amplitude under non-saturating conditions (mw power, 0.2 μW). The horizontal line corresponds to the temperature dependence described by the Curie law (no low-lying excited states).

DSD. The temperature dependence of the EPR amplitude (Figure 4b) shows a nearly exclusive population of the $S = {}^1/_2$ ground state at the temperatures below 15 K. The temperature dependence presented in Figure 4b is typical of $[4Fe\text{-}4S]^+$ clusters and can be used to obtain information about the energies and multiplicities of the excited states.[40] Spin quantification of the reduced, EPR active clusters revealed that the $[4Fe\text{-}4S]^+$/protein concentration ratio is ∼56%. In contrast, cluster quantification on a different sample conducted using the ferrozine assay to assess iron content yielded a level of incorporation of 73.5%. Such a difference could be explained by the challenge of completely reducing the clusters in the EPR sample.

To obtain additional proof of the pairwise binding of the [4Fe-4S] clusters to the DSD protein, we used the pulsed electron−electron double-resonance (ELDOR) technique that detects a magnetic dipole interaction between the paramagnetic centers.[41] Pulsed ELDOR and related techniques are routinely used to determine the distances between paramagnetic centers (spin-labels, native radicals, and/or metal centers) in biological systems.[42−49] In particular, pulsed ELDOR was employed to study the electron transfer systems containing [Fe-S] clusters and to obtain information about the relative spatial arrangement of the electron transfer carriers and the electronic structure of the [Fe-S] clusters themselves.[43,50,51]

In the pulsed ELDOR experiment, the pumping mw frequency, ν_{pmp}, was set in resonance with the maximum of the ESE field sweep spectrum (g_y position). The observation frequency, ν_{obs}, was 93 MHz higher, which corresponds to the observation EPR position shifted by ∼3.3 mT toward g_z (Figure

dx.doi.org/10.1021/bi401199s | Biochemistry 2013, 52, 7586−7594

5a). Because the characteristic width of the EPR spectrum (~17 mT) is much greater than the pumping mw excitation width

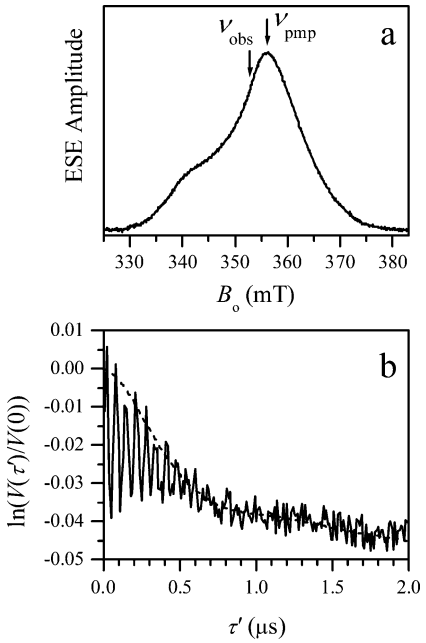

Figure 5. (a) Two-pulse ESE field sweep spectrum of reduced DSD-bis[4Fe-4S]. Experimental conditions: mw frequency, 9.640 GHz; mw pulses, 15 and 20 ns; time interval between the mw pulses (τ), 200 ns; temperature, 10 K. (b) The solid trace is the experimental pulsed ELDOR trace obtained using the three-pulse sequence. Experimental conditions: ν_{obs} = 9.733 GHz; ν_{pmp} = 9.640 GHz; B_o = 356.1 mT (EPR signal maximum for ν_{pmp}); observation mw pulses, 15 and 20 ns; pumping mw pulse, 12 ns; temperature, 10 K. To suppress the residual ^{1}H ESEEM, the time interval between the observation pulses, τ, was varied from 2 to 2.3 μs with a step of 10 ns, and the ELDOR traces were summed. The dashed trace is a numerical simulation (see the text for details).

(~1.5 mT for the 12 ns pumping mw pulse), the ELDOR effect was expected to be very small, especially taking into account the incomplete pairing of the EPR active $[4Fe\text{-}4S]^+$ clusters and possible (and unpredictable) orientational selectivity effects. With a distance between the [4Fe-4S] cluster binding sites of ~30 Å in the model, the dipole interaction constant was not expected to be very large, less than ~4 MHz (see below). Therefore, we have used in our experiments the three-pulse ELDOR sequence (based on the two-pulse observation sequence),[41] which offers somewhat better sensitivity than the four-pulse sequence.[52] The pulsed ELDOR measurements were performed at 15 K, where the population of the excited states is still negligible (see Figure 4b), but the longitudinal relaxation time is already short enough to allow the measurements with a reasonably fast pulse repetition rate of 500 Hz.

The experimental ELDOR trace is presented in Figure 5 (solid trace). It exhibits the oscillations with a high frequency of ~15 MHz (~70 ns period), which represent a residual electron spin echo envelope modulation (ESEEM) at the Zeeman frequency of ^{1}H. Such a residual ESEEM is often observed in ELDOR experiments with an insufficient frequency separation between ν_{obs} and ν_{pmp}.[44] In addition, a fast-damping low-frequency oscillation is observed with the first minimum at a τ' of ~700 ns (where τ' is the time interval between the first observation pulse and the pumping pulse). This oscillation arises from the dipole interaction between the $[4Fe\text{-}4S]^+$ clusters, which follows from the facts that the $[4Fe\text{-}4S]^+$ clusters exist only as a protein-bound species and no such oscillation was observed for the samples with low $[4Fe\text{-}4S]^+$/protein concentration ratios, resulting in a negligible probability of pair formation.

The characteristic frequency of the low-frequency oscillation assigned to the dipole interaction between the clusters is only ~0.7 MHz (as estimated from the position of the first minimum). In a point dipolar approximation, this dipole interaction would correspond to a distance of ~42 Å, significantly longer than the structurally reasonable distance of ~30−34 Å. The dashed trace in Figure 5 shows the simulation (using a simple point dipolar model and neglecting any possible orientational selectivity) for the uniform distance distribution from 36.5 to 51.5 Å ($\langle R\rangle$ = 44 Å; ΔR = 15 Å). The simulated pairwise effect is superimposed on the exponential decay from the uniformly distributed spins.

To explain this discrepancy, one has to take into account that the $[4Fe\text{-}4S]^+$ clusters represent mixed valence systems, with the total dipole interaction being a weighted sum of the contributions of the interactions between the individual ions.[43,50,51] Therefore, representing the whole cluster by a single point dipole is not appropriate, and the spins of the individual ions and the way they are coupled together have to be considered explicitly. The spin coupling scheme for the $[4Fe\text{-}4S]^+$ cluster was described elsewhere.[53] Briefly, the total spin S of $^1/_2$ results from antiferromagnetic coupling of two pairs of ferromagnetically coupled ions, Fe(II)−Fe(II) (S = 4) and Fe(II)−Fe(III) ($S = {}^9/_2$). The spin projection factors that determine the statistical weights of individual dipole interactions are $-{}^4/_3$ for the ions of the Fe(II)−Fe(II) pair and $^{11}/_6$ for the ions of the Fe(II)−Fe(III) pair (the iron ions in this pair are actually equivalent and have a charge of 2.5). The dipole interaction between two $[4Fe\text{-}4S]^+$ clusters depends on their relative orientation. To make a simple estimate of the overall range of the possible dipole interaction constants, we will use the fact that the distance between the clusters (~30 Å) is ~1 order of magnitude greater than the cluster size (cube side of ~2.5 Å) and will write for the dipole interaction constant[51,52]

$$D \approx \sum_{i,j} K_i K_j \frac{g_i g_j \beta^2}{R_{ij}^3}$$

where K_i and K_j are the spin projection factors of Fe ions in the different clusters, g_i and g_j are their g values, respectively, β is the Bohr magneton, R_{ij} is the distance between ions i and j, and all of the $\mathbf{R}_{ij}$ vectors are thought to be collinear. Then, with the minimal and maximal R_{ij} values equal to ~30 and 35 Å, respectively, one can easily estimate the minimal and maximal possible D values: $D_{min} \approx 0.4$ MHz, and $D_{max} \approx 5.2$ MHz. The values close to D_{min} are realized for the clusters oriented in such a way that the Fe(II)−Fe(II) pair of one cluster is the closest to the other cluster. The values close to D_{max} are realized when Fe(II)−Fe(III) pairs of the clusters are closest to each other (at 30 Å), while their Fe(II)−Fe(II) pairs are at a maximal separation (35 Å).

The observed ELDOR oscillation frequency of ~0.7 MHz is closer to the lower limit of the estimated range of dipole interactions, which indicates that the clusters are approximately oriented by the Fe(II)−Fe(II) pairs toward each other. These

dx.doi.org/10.1021/bi401199s | Biochemistry 2013, 52, 7586−7594

considerations demonstrate that the interpretation of the observed dipole interaction between mixed-valence systems in terms of distance requires additional information about the internal electronic structure and relative orientation of the centers.

CONCLUSIONS

In this work, we exploited the pseudo-2-fold symmetry of DSD, a *de novo*-designed dimeric three-helix bundle, to generate a model protein that contains two iron−sulfur clusters in the hydrophobic core. Starting with the primary coordination sphere of a natural [4Fe-4S] cuboidal cluster, we replaced leucines in the three-helix bundle with coordinating cysteines in the appropriate side chain rotamers to satisfy cluster coordination. The substitutions result in the formation of a hydrophilic cavity in the protein core, which is then filled by insertion of the cluster. Our data show that the mutations are structurally conservative, resulting in highly helical dimeric proteins in the apo and holo states. The folding stability of the proteins is found to increase in the following order: DSD-4Cys < DSD-bis[4Fe-4S] < DSD (mirroring the trend in core hydrophobicity and packing). Further, we showed that DSD-bis[4Fe-4S] contains two intact cubane iron−sulfur clusters located at the intended distance. EPR and ELDOR data are consistent with the expected distance of 29−34 Å, derived from the model.

The design approach adopted here replaces the hydrophobic core of a scaffold protein with a sterically compatible metal binding center and has been validated in several systems.[19,21,54−63] Helical systems derived from the coiled coil motif have proven to be particularly adept in accommodating metal binding sites, because the interhelix distances in the core are compatible with the typical bond length in metal−ligand complexes. The regular structure repeat of the coiled coil lends itself to parametrization and thus to computational design; further, the structure repeat is reflected at the sequence level in a motif of seven amino acids that fold in a full helical turn, named the heptad repeat.[27] Thus, a metal binding site can be easily moved along the longitudinal axis of the scaffold simply by replicating the sequence motif in a modular fashion. Here, we demonstrated the incorporation of those design principles in a model system that contains two clusters at a fixed distance, estimated to be 29−34 Å. Although this distance is not conductive to efficient electron tunneling, the design principles described here could be extended to modulate intercluster distances by repositioning the motif containing the cluster coordinating cysteines along the longitudinal axis of DSD. Further, this procedure may be used to add additional metal binding sites or extended to other three-helix bundle scaffolds.

ASSOCIATED CONTENT

Supporting Information

Gel filtration elution profile, analytical ultracentrifugation data, dipole interaction estimates, cyclic voltammetry, and protein modeling. This material is available free of charge via the Internet at http://pubs.acs.org.

AUTHOR INFORMATION

Corresponding Author

*E-mail: gghirlanda@asu.edu. Telephone: (480) 965-6645.

Funding

This work is supported by the Center for Bio-Inspired Solar Fuel Production, an Energy Frontier Research Center funded by the U.S. Department of Energy, Office of Science, Office of Basic Energy Sciences, via Grant DE-SC0001016. The EPR Facility at the University of Arizona was supported by National Science Foundation Grants BIR-9224431, DBI-9604939, and DBI-0139459 for construction of the variable-frequency pulsed EPR spectrometers, by National Institutes of Health Grant RR020959 for the purchase of the 2T electromagnet, and by National Center for Research Resources Grant 1S10RR26416-01 for acquisition of the Bruker Elexsys E500 EPR spectrometer.

Notes

The authors declare no competing financial interest.

ACKNOWLEDGMENTS

We thank the Arizona State University Proteomics Facility for MALDI access, John Schulze (Proteomics Department, University of California, Davis, CA) for amino acid analysis, and Dr. Chad K. Park (Analytical Biophysical Facility, University of Arizona) for performing analytical ultracentrifugation.

ABBREVIATIONS

CD, circular dichroism; EPR, electron paramagnetic resonance; ELDOR, electron−electron double-resonance spectroscopy; TIS, triisopropylsilane; TFA, trifluoroacetic acid; BME, β-mercaptoethanol; TCEP, tris(2-carboxyethyl)phosphine hydrochloride.

REFERENCES

(1) Lill, R. (2009) Function and biogenesis of iron-sulphur proteins. *Nature 460*, 831−838.

(2) Beinert, H., Holm, R. H., and Münck, E. (1997) Iron-sulfur clusters: Nature's modular, multipurpose structures. *Science 277*, 653−659.

(3) Meyer, J. (2008) Iron-sulfur protein folds, iron-sulfur chemistry, and evolution. *JBIC, J. Biol. Inorg. Chem. 13*, 157−170.

(4) Eck, R. V., and Dayhoff, M. O. (1966) Evolution of the structure of ferredoxin based on living relics of primitive amino acid sequences. *Science 152*, 363−366.

(5) Hinchliffe, P., and Sazanov, L. A. (2005) Organization of iron-sulfur clusters in respiratory complex I. *Science 309*, 771−774.

(6) Sazanov, L. A., and Hinchliffe, P. (2006) Structure of the hydrophilic domain of respiratory complex I from *Thermus thermophilus*. *Science 311*, 1430−1436.

(7) Jordan, P., Fromme, P., Witt, H. T., Klukas, O., Saenger, W., and Krauss, N. (2001) Three-dimensional structure of cyanobacterial photosystem I at 2.5 Å resolution. *Nature 411*, 909−917.

(8) Peters, J., Lanzilotta, W., Lemon, B., and Seefeldt, L. (1998) X-ray crystal structure of the Fe-only hydrogenase (Cpl) from *Clostridium pasteurianum* to 1.8 Å resolution. *Science 282*, 1853−1858.

(9) Fontecilla-Camps, J. C., Volbeda, A., Cavazza, C., and Nicolet, Y. (2007) Structure/function relationships of [NiFe]- and [FeFe]-hydrogenases. *Chem. Rev. 107*, 4273−4303.

(10) Krishna, S. S., Sadreyev, R. I., and Grishin, N. V. (2006) A tale of two ferredoxins: Sequence similarity and structural differences. *BMC Struct. Biol. 6*, 8−12.

(11) Antonkine, M. L., and Golbeck, J. H. (2006) Molecular Interactions of the Stromal Subunit PsaC with the PsaA/PsaB Heterodimer. In *Photosystem I: The Light-Driven Plastocyanin:Ferredoxin Oxidoreductase* (Golbeck, J. H., Ed.) pp 79−98, Springer, New York.

(12) Mulder, D. W., Shepard, E. M., Meuser, J. E., Joshi, N., King, P. W., Posewitz, M. C., Broderick, J. B., and Peters, J. W. (2011) Insights

into [FeFe]-hydrogenase structure, mechanism, and maturation. *Structure 19*, 1038−1052.
(13) Nicolet, Y., Piras, C., Legrand, P., Hatchikian, C. E., and Fontecilla-Camps, J. C. (1999) *Desulfovibrio desulfuricans* iron hydrogenase: The structure shows unusual coordination to an active site Fe binuclear center. *Struct. Folding Des. 7*, 13−23.
(14) Dubini, A., Mus, F., Seibert, M., Grossman, A. R., and Posewitz, M. C. (2009) Flexibility in anaerobic metabolism as revealed in a mutant of *Chlamydomonas reinhardtii* lacking hydrogenase activity. *J. Biol. Chem. 284*, 7201−7213.
(15) Scott, M. P., and Biggins, J. (1997) Introduction of a [4Fe-4S (S-cys)4]$^{+1,+2}$ iron-sulfur center into a four-α helix protein using design parameters from the domain of the Fx cluster in the Photosystem I reaction center. *Protein Sci. 6*, 340−346.
(16) Antonkine, M. L., Maes, E. M., Czernuszewicz, R. S., Breitenstein, C., Bill, E., Falzone, C., Balasubramanian, R., Lubner, C. E., Bryant, D. A., and Golbeck, J. H. (2007) Chemical rescue of a site-modified ligand to a [4Fe−4S] cluster in PsaC, a bacterial-like dicluster ferredoxin bound to Photosystem I. *Biochim. Biophys. Acta 1767*, 712−724.
(17) Antonkine, M. L., Koay, M. S., Epel, B., Breitenstein, C., Gopta, O., Gärtner, W., Bill, E., and Lubitz, W. (2009) Synthesis and characterization of de novo designed peptides modelling the binding sites of [4Fe-S] clusters in photosystem I. *Biochim. Biophys. Acta 1787*, 995−1008.
(18) Kennedy, M. L., and Gibney, B. R. (2002) Proton coupling to [4Fe-4S]$^{2+/+}$ and [4Fe-4Se]$^{2+/+}$ oxidation and reduction in a designed protein. *J. Am. Chem. Soc. 124*, 6826−6827.
(19) Grzyb, J., Xu, F., Weiner, L., Reijerse, E. J., Lubitz, W., Nanda, V., and Noy, D. (2010) De novo design of a non-natural fold for an iron-sulfur protein: α-Helical coiled-coil with a four-iron four-sulfur cluster binding site in its central core. *Biochim. Biophys. Acta 1797*, 406−413.
(20) Grzyb, J., Xu, F., Nanda, V., Luczkowska, R., Reijerse, E., Lubitz, W., and Noy, D. (2012) Empirical and computational design of iron-sulfur cluster proteins. *Biochim. Biophys. Acta 1817*, 1256−1262.
(21) Coldren, C. D., Hellinga, H. W., and Caradonna, J. P. (1997) The rational design and construction of a cuboidal iron-sulfur protein. *Proc. Natl. Acad. Sci. U.S.A. 94*, 6635−6640.
(22) Laplaza, C. E., and Holm, R. H. (2001) Helix-loop-helix peptides as scaffolds for the construction of bridged metal assemblies in proteins: The spectroscopic A-cluster structure in carbon monoxide dehydrogenase. *J. Am. Chem. Soc. 123*, 10255−10264.
(23) Gibney, B. R., Mulholland, S. E., Rabanal, F., and Dutton, P. L. (1996) Ferredoxin and ferredoxin-heme maquettes. *Proc. Natl. Acad. Sci. U.S.A. 93*, 15041−15046.
(24) Roy, A., Madden, C., and Ghirlanda, G. (2012) Photo-induced hydrogen production in a helical peptide incorporating a [FeFe] hydrogenase active site mimic. *Chem. Commun. 48*, 9816−9818.
(25) Faiella, M., Roy, A., Sommer, D. J., and Ghirlanda, G. (2013) Design of functional proteins: Towards artificial hydrogenases. *Biopolymers*, DOI: 10.1002/bip.22420.
(26) Woolfson, D. N., Bartlett, G. J., Bruning, M., and Thomson, A. R. (2012) New currency for old rope: From coiled-coil assemblies to α-helical barrels. *Curr. Opin. Struct. Biol. 22*, 432−441.
(27) Crick, F. H. C. (1953) The packing of α-helices: Simple coiled-coils. *Nature 6*, 689−697.
(28) DeLano, W. L. (2005) *MacPymol: A PyMol-based Molecular Graphics Application for MacOS X*, DeLano Scientific, LLC, South San Francisco.
(29) Laurie, A. T. R., and Jackson, R. M. (2005) Q-SiteFinder: An energy-based method for the prediction of protein-ligand binding sites. *Bioinformatics 21*, 1908−1916.
(30) Astashkin, A. V., Enemark, J. H., and Raitsimring, A. (2006) 26.5−40 GHz Ka-band pulsed EPR spectrometer. *Concepts Magn. Reson. 29B*, 125−136.
(31) Hoppe, A., Pandelia, M.-E., Gärtner, W., and Lubitz, W. (2011) [Fe_4S_4]- and [Fe_3S_4]-cluster formation in synthetic peptides. *Biochim. Biophys. Acta 1807*, 1414−1422.
(32) Carter, P. (1971) Spectrophotometric determination of serum iron at the submicrogram level with a new reagent (ferrozine). *Anal. Biochem. 40*, 450−458.
(33) Han, G. W., Yang, X. L., McMullan, D., Chong, Y. E., Krishna, S. S., Rife, C. L., Weekes, D., Brittain, S. M., Abdubek, P., Ambing, E., Astakhova, T., Axelrod, H. L., Carlton, D., Caruthers, J., Chiu, H. J., Clayton, T., Duan, L., Feuerhelm, J., Grant, J. C., Grzechnik, S. K., Jaroszewski, L., Jin, K. K., Klock, H. E., Knuth, M. W., Kumar, A., Marciano, D., Miller, M. D., Morse, A. T., Nigoghossian, E., Okach, L., Paulsen, J., Reyes, R., van den Bedem, H., White, A., Wolf, G., Xu, Q., Hodgson, K. O., Wooley, J., Deacon, A. M., Godzik, A., Lesley, S. A., Elsliger, M. A., Schimmel, P., and Wilson, I. A. (2010) Structure of a tryptophanyl-tRNA synthetase containing an iron-sulfur cluster. *Acta Crystallogr. F66*, 1326−1334.
(34) Beinert, H. (2000) Iron-sulfur proteins: Ancient structures, still full of surprises. *JBIC, J. Biol. Inorg. Chem. 5*, 2−15.
(35) Koay, M. S., Antonkine, M. L., Gärtner, W., and Lubitz, W. (2008) Modelling low-potential [Fe4S4] clusters in proteins. *Chem. Biodiversity 5*, 1571−1587.
(36) Sweeney, W. V., and Rabinowitz, J. C. (1980) Proteins containing 4Fe-4S clusters: An overview. *Annu. Rev. Biochem. 49*, 139−161.
(37) Jin, Z., Heinnickel, M., Krebs, C., Shen, G., Golbeck, J. H., and Bryant, D. A. (2008) Biogenesis of Iron-Sulfur Clusters in Photosystem I: Holo-NfuA from the Cyanobacterium *Synechococcus* sp. PCC 7002 Rapidly and Efficiently Transfers [4Fe-4S] Clusters to Apo-PsaC in vitro. *J. Biol. Chem. 283*, 28426−28435.
(38) Bertini, I., Gray, H. B., Lippard, S. J., and Valentine, J. S. (1994) *Bioinorganic chemistry*, University Science Books, Sausalito, CA.
(39) Ogihara, N. L., Ghirlanda, G., Bryson, J. W., Gingery, M., DeGrado, W. F., and Eisenberg, D. (2001) Design of three-dimensional domain-swapped dimers and fibrous oligomers. *Proc. Natl. Acad. Sci. U.S.A. 98*, 1404−1409.
(40) Papaefthymiou, G. C., Frankel, R. B., and Foner, S. (1980) Magnetic Properties of [$Fe_4S_4(SR)_4$]$^{3-}$ Clusters. *J. Phys. (Paris) 41*, C493−C494.
(41) Milov, A. D., Marayasov, A. G., and Tsvetkov, Y. D. (1998) Pulsed electron double resonance (PELDOR) and its applications in free-radicals research. *Appl. Magn. Reson. 15*, 107−143.
(42) Schiemann, O., and Prisner, T. F. (2007) Long-range distance determinations in biomacromolecules by EPR spectroscopy. *Q. Rev. Biophys. 40*, 1−53.
(43) Astashkin, A. V., Seravalli, J., Mansoorabadi, S. O., Reed, G. H., and Ragsdale, S. W. (2006) Pulsed electron paramagnetic resonance experiments identify the paramagnetic intermediates in the pyruvate ferredoxin oxidoreductase catalytic cycle. *J. Am. Chem. Soc. 128*, 3888−3889.
(44) Jeschke, G. (2012) DEER Distance Measurements on Proteins. In *Annual Review of Physical Chemistry* (Johnson, M. A., and Martinez, T. J., Eds.) Vol. *63*, pp 419−446, Annual Reviews, Palo Alto, CA.
(45) Swanson, M. A., Kathirvelu, V., Majtan, T., Frerman, F. E., Eaton, G. R., and Eaton, S. S. (2009) DEER Distance Measurement Between a Spin Label and a Native FAD Semiquinone in Electron Transfer Flavoprotein. *J. Am. Chem. Soc. 131*, 15978−15985.
(46) Sen, K. I., Wu, H., Backer, J. M., and Gerfen, G. J. (2010) The Structure of p85ni in Class IA Phosphoinositide 3-Kinase Exhibits Interdomain Disorder. *Biochemistry 49*, 2159−2166.
(47) Astashkin, A. V., Rajapakshe, A., Cornelison, M. J., Johnson-Winters, K., and Enemark, J. H. (2012) Determination of the Distance between the Mo(V) and Fe(III) Heme Centers of Wild Type Human Sulfite Oxidase by Pulsed EPR Spectroscopy. *J. Phys. Chem. B 116*, 1942−1950.
(48) Gordon-Grossman, M., Kaminker, I., Gofman, Y., Shai, Y., and Goldfarb, D. (2011) W-Band pulse EPR distance measurements in peptides using Gd^{3+}-dipicolinic acid derivatives as spin labels. *Phys. Chem. Chem. Phys. 13*, 10771−10780.
(49) Lovett, J. E., Bowen, A. M., Timmel, C. R., Jones, M. W., Dilworth, J. R., Caprotti, D., Bell, S. G., Wong, L. L., and Harmer, J.

(2009) Structural information from orientationally selective DEER spectroscopy. *Phys. Chem. Chem. Phys. 11*, 6840−6848.
(50) Elsasser, C., Brecht, M., and Bittl, R. (2002) Pulsed electron-electron double resonance on multinuclear metal clusters: Assignment of spin projection factors based on the dipolar interaction. *J. Am. Chem. Soc. 124*, 12606−12611.
(51) Elsaesser, C., Brecht, M., and Bittl, R. (2005) Treatment of spin-coupled metal-centres in pulsed electron-electron double-resonance experiments. *Biochem. Soc. Trans. 33*, 15−19.
(52) Martin, R. E., Pannier, M., Diederich, F., Gramlich, V., Hubrich, M., and Spiess, H. W. (1998) Determination of end-to-end distances in a series of TEMPO diradicals of up to 2.8 nm length with a new four-pulse double electron electron resonance experiment. *Angew. Chem., Int. Ed. 37*, 2834−2837.
(53) Torres, R. A., Lovell, T., Noodleman, L., and Case, D. A. (2003) Density functional and reduction potential calculations of Fe4S4 clusters. *J. Am. Chem. Soc. 125*, 1923−1936.
(54) Zastrow, M. L., Peacock, A. F. A., Stuckey, J. A., and Pecoraro, V. L. (2011) Hydrolytic catalysis and structural stabilization in a designed metalloprotein. *Nat. Chem.*, 1−6.
(55) Salgado, E. N., Radford, R. J., and Tezcan, F. A. (2010) Metal-directed protein self-assembly. *Acc. Chem. Res. 43*, 661−672.
(56) Cordova, J. M., Noack, P. L., Hilcove, S. A., Lear, J. D., and Ghirlanda, G. (2007) Design of a functional membrane protein by engineering a heme-binding site in glycophorin A. *J. Am. Chem. Soc. 129*, 512−518.
(57) Shinde, S., Cordova, J. M., Woodrum, B. W., and Ghirlanda, G. (2012) Modulation of function in a minimalist heme-binding membrane protein. *JBIC, J. Biol. Inorg. Chem. 17*, 557−564.
(58) Calhoun, J. R., Nastri, F., Maglio, O., Pavone, V., Lombardi, A., and Degrado, W. F. (2005) Artificial diiron proteins: From structure to function. *Biopolymers 80*, 264−278.
(59) Shiga, D., Funahashi, Y., Masuda, H., Kikuchi, A., Noda, M., Uchiyama, S., Fukui, K., Kanaori, K., Tajima, K., Takano, Y., Nakamura, H., Kamei, M., and Tanaka, T. (2012) Creation of a binuclear purple copper site within a de novo coiled-coil protein. *Biochemistry 51*, 7901−7907.
(60) Chakraborty, S., Iranzo, O., Zuiderweg, E. R. P., and Pecoraro, V. L. (2012) Experimental and theoretical evaluation of multisite cadmium(II) exchange in designed three-stranded coiled-coil peptides. *J. Am. Chem. Soc. 134*, 6191−6203.
(61) Der, B. S., Machius, M., Miley, M. J., Mills, J. L., Szyperski, T. A., and Kuhlman, B. (2012) Metal-mediated affinity and orientation specificity in a computationally designed protein homodimer. *J. Am. Chem. Soc. 134*, 375−385.
(62) Ghirlanda, G. (2009) Design of membrane proteins: Toward functional systems. *Curr. Opin. Chem. Biol. 13*, 643−651.
(63) Ghirlanda, G., Osyczka, A., Liu, W., Antolovich, M., Smith, K. M., Dutton, P. L., Wand, A. J., and Degrado, W. F. (2004) De novo design of a D2-symmetrical protein that reproduces the diheme four-helix bundle in cytochrome bc_1. *J. Am. Chem. Soc. 126*, 8141−8147.